

## Article

# Finite-Element Analysis on Energy Dissipation and Sealability of Premium Connections under Dynamic Loads

Yang Yu <sup>1</sup>, Yinping Cao <sup>2,\*</sup> , Zhan Qu <sup>1,3,\*</sup>, Yihua Dou <sup>2</sup> and Zidi Wang <sup>2</sup><sup>1</sup> School of Aeronautics, Northwestern Polytechnical University, Xi'an 710072, China; yuyang029xian@163.com<sup>2</sup> Mechanical Engineering College, Xi'an Shiyou University, Xi'an 710065, China; yhdou@vip.sina.com (Y.D.); wangzidi555@163.com (Z.W.)<sup>3</sup> College of Petroleum Engineering, Xi'an Shiyou University, Xi'an 710065, China

\* Correspondence: yuyxysy@163.com or caoyinping029@163.com (Y.C.); zhqu@xsyu.edu.cn (Z.Q.)

**Abstract:** In the process of high flow rate fracture and high gas production, the sealing performance of the premium connection decreases due to the dynamic load and vibration of downhole tubing strings, which may cause accidents. Existing static analysis methods cannot effectively explain this phenomenon. The main objective of this paper is to propose a novel analytical method for evaluating the sealing performance of a premium connection. In this paper, a dynamic model of sealing surfaces of the premium connection is established based on the vibration equation of elastic rod, and the hysteresis characteristics and energy dissipation mechanism of sealing surfaces are analyzed. Considering the influence of spherical radius, internal pressure, axial cyclic load amplitude, and modal vibration, a spherical-conical premium connection finite element model is established to analyze the influence laws of the connection's energy dissipation and sealing performance. The results show that the sealing performance of the premium connection under dynamic load can be effectively analyzed by using energy dissipation theory compared with traditional static contact analysis. Compared with the vibration of the tubing string, the dynamic loads caused by the change of fluid pressure and flow rate in the tubing string have a significant influence on the connection's sealing performance. When the internal pressure and axial cyclic loads are 80 MPa, 400 kN, or 60 MPa and 500 kN respectively, serious plastic deformation occurs in the thread and sealing surfaces, and the energy dissipation of the sealing surfaces increases significantly, which could lead to sealing failure.

**Keywords:** premium connection; energy dissipation; dynamic load; modal vibration; finite element model



**Citation:** Yu, Y.; Cao, Y.; Qu, Z.; Dou, Y.; Wang, Z. Finite-Element Analysis on Energy Dissipation and Sealability of Premium Connections under Dynamic Loads. *Processes* **2023**, *11*, 1927. <https://doi.org/10.3390/pr11071927>

Academic Editors: Tianshou Ma and Yuqiang Xu

Received: 18 May 2023

Revised: 23 June 2023

Accepted: 24 June 2023

Published: 26 June 2023



**Copyright:** © 2023 by the authors. Licensee MDPI, Basel, Switzerland. This article is an open access article distributed under the terms and conditions of the Creative Commons Attribution (CC BY) license (<https://creativecommons.org/licenses/by/4.0/>).

## 1. Introduction

The premium connection serves as the connection structure for downhole tubing, connecting tubing to thousands of meters of the tubing string. As shown in Figure 1, the premium connection consists mainly of sealing surfaces, torque shoulders, and threads. The sealing surface is the main sealing structure, the torque shoulder has the function of resisting torque overload and auxiliary sealing, and the threads are used to connect the tubing. Connections are the most dangerous part of the tubing string. Due to complex downhole loads, connections leak frequently and even lead to accidents [1,2]. According to field statistics, connection failure accounts for 85–95% [3,4] of all tubing string failures. Earlier research on the premium connection was mainly based on static load, and the sealing performance was studied by analyzing the equivalent stress, contact pressure, and contact length of the connection. Li et al. [5] used a combination of experimental and theoretical research to study the friction characteristics of bolted connection interfaces. Xu et al. [6–8] used a combination of finite element simulation and theoretical models to calculate the contact pressure and contact area of the sealing surfaces, taking into account the micro profile of the sealing surfaces. The relationship between the average contact pressure,

circumferential leakage width, and sealing surfaces was obtained. Nasraoui et al. [9] constructed a simplified numerical model of bolt bonding surfaces and established a contact stiffness matrix. Xu et al. [10] established contact pressure distribution and sealing surfaces length of premium connection under different buckling torques by analytical method and further evaluated the sealing condition of the connection by a comprehensive consideration of various factors. Zhiqian et al. [11] analyzed the sealing performance of the connection by combining the elastic-plastic mechanical contact theory and calculated geometric morphology parameters of the rough surfaces. Chen et al. [12,13] analyzed the effect of preload on the threaded seal and the influence of contact stress at threads, sealing surfaces and shoulders on the sealing performance.

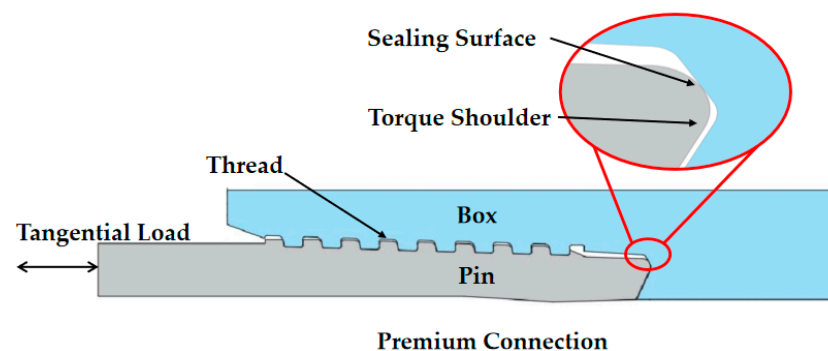


**Figure 1.** Schematic diagram of the spherical-conical premium connection.

Affected by loads such as the weight of tubing string, internal and external fluid pressure, viscous damping when fluid flows in tubing string and Coulomb friction force, premium connections are subjected to loads such as axial force, internal and external pressure, bending moment, etc. During high flow rate fracturing and high production gas operation, the dynamic load change of tubing caused by the change of fluid pressure and flow rate in tubing causes vibration of tubing [14–16]. Under dynamic load, the sealing surfaces will slip cyclically, resulting in connection loosening or poor sealing performance. However, the traditional static contact analysis method cannot effectively explain this problem. As shown in Figure 1, the sealing surfaces can be considered as two contact surfaces, which are mainly subjected to normal and tangential loads. Normal loads are generated by the interference fit of sealing surfaces and internal and external pressure, which affect contact morphology and pressure of sealing surfaces. Tangential loads are generated by the axial force of the tubing strings and will cause the horizontal slip of the sealing surfaces. Under cyclic loading, the sealing surfaces of premium connections will undergo microslip or gross slip, which will lead to energy dissipation in the structural system [17,18]. As shown in Figure 2, under the action of external incremental load, microslip (stick and slip coexist) occurs on the sealing surfaces, and the slope of the force-displacement curve decreases gradually, resulting in stiffness degradation. As the load increases further, gross slip occurs on the sealing surfaces. At this time, the force-displacement curve approaches the level and the force remains constant, and the gross slip increases gradually [19]. As shown in Figure 3, under cyclic loading, the microslip and gross slip are converted into each other during loading and unloading, resulting in force-displacement hysteresis [17,20,21]. The area of the force-displacement hysteresis curve is the energy dissipation generated during a cycle of loading [22]. Loosening of the connection can be explained by the phenomenon of force-displacement hysteresis of contact surfaces. In the early stage, Iwan [23] built an energy dissipation model of bolted connections based on spring-damped vibration theories. Wang et al. [24] optimized the Iwan model to apply it to the study of energy dissipation in more complex situations. Zhang et al. [25,26] studied the normal stiffness, normal damping, and energy dissipation of the bolt bonding surfaces under different external loads.

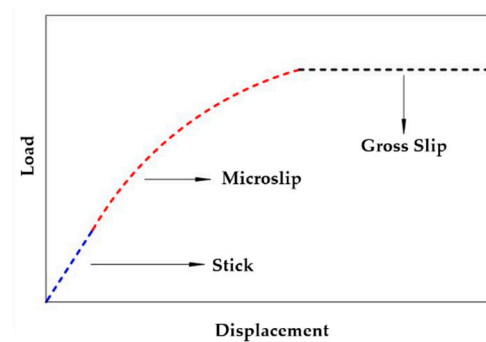


**Figure 2.** Force–displacement curve of sealing surfaces under single increased load.

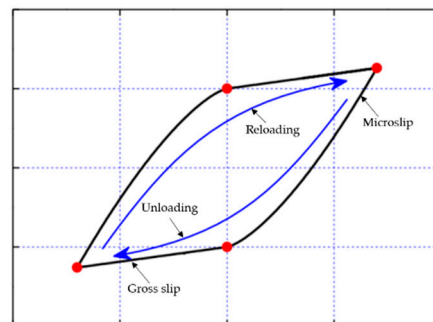


**Figure 3.** Sealing surfaces force–displacement hysteresis curve under cyclic load.

The premium connection has more complex geometry and load conditions than the bolted joint. At present, there are fewer reports about the sealing property of premium connections under dynamic load. Yang et al. [10] established a contact stress model of sealing surfaces and analyzed the energy dissipation law under different sealing concinities. Yu et al. [27] established a shear layer microslip model of the sealing surfaces at an early stage and analyzed the influence of the shear layer coefficient on the microslip state and energy dissipation of the sealing surfaces. Yu et al. [28]. studied the sealing performance of special threaded joints from a micro level, and based on fractal contact theory, analyzed the effects of fractal dimension and amplitude coefficient on the contact behavior of rough surfaces. The above researches provide some new ideas for the sealing analysis of premium connection, but the results are limited by simplifying models and assuming conditions, such as ignoring the threads and torque shoulders.

In summary, to address the limitations of existing sealing performance evaluation methods, this paper considers the influence of threads and torque shoulders on the contact pressure of the sealing surface of premium connections. On the basis of the traditional evaluation of sealing performance, energy dissipation theory is added to evaluate the sealing performance of premium connections under dynamic loads. We analyze the impact of different parameters on sealing performance under different working conditions based on energy dissipation values. Firstly, based on the vibration equation of the elastic rod, a dynamic model of the connection sealing surfaces is established to analyze the energy dissipation mechanism. Then, based on friction contact analysis and vibration mode analysis, a finite element model (FEM) of spherical-conical premium connection is established by ABQUS numerical simulation software. Finally, the influence of different spherical radii, internal pressure, axial cyclic load amplitudes, and modal shapes on energy dissipation and sealing performance of premium connection under dynamic load is analyzed. The sealing performance evaluation method established based on the energy dissipation theory can provide technical guidance for the design of spherical-conical premium connections and serve as a reference basis for selecting suitable premium connections on oilfield construction sites.

## 2. Materials and Methods

The energy dissipation of the sealing surfaces is reflected by the force–displacement hysteresis curve. In order to obtain the force–displacement hysteresis curve, a non-linear vibration model of the sealing surfaces must be established first. As shown in Figure 4, the two sealing surfaces of the Pin and the Box are simplified to an elastic rod and a rigid body, respectively, and the contact slip behavior between them is represented by a shear layer without thickness.

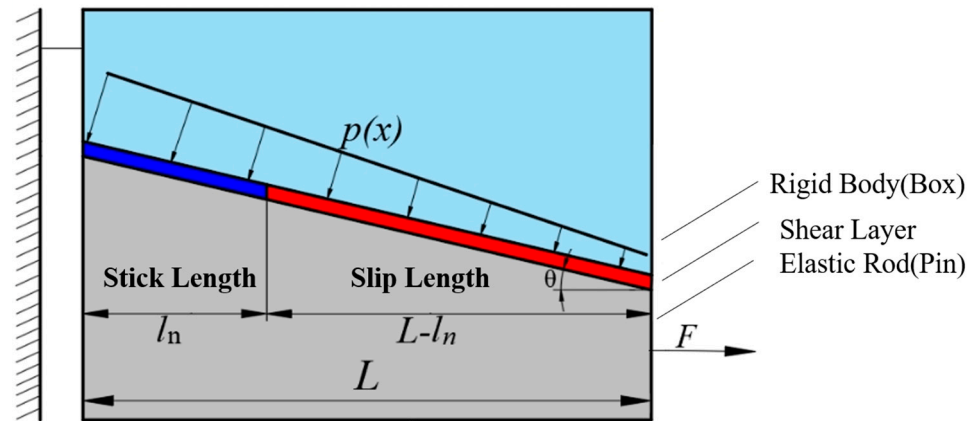


**Figure 4.** Contact slip model of sealing surfaces.

### 2.1. Dynamic Model Establishment

Based on the vibration balance equation of the rod, the governing balance equations for the stick and slip regions can be obtained as [18,27]:

Stick regions:

$$EAu''(x) - ku(x) \cos \theta = 0, 0 \leq x \leq l_n \quad (1)$$

Microslip regions:

$$EAu''(x) - \mu p(x) \cos \theta = 0, l_n \leq x \leq L \quad (2)$$

Boundary conditions:

$$EAu'(0) = 0 \quad EA'(L) = F \quad (3)$$

The continuity conditions satisfied at the stick and slip boundary positions,  $x = l_n$ , is:

$$u(l_n)^- = u(l_n)^+ \quad u'(l_n)^- = u'(l_n)^+ \quad (4)$$

In equation:

$E$ —is the Elastic modulus of elastic rod, GPa;

$A$ —is the section area of the elastic rod,  $\text{mm}^2$ ;

$\theta$ —is the taper of the sealing surface,  $^\circ$ ;

$k$ —is the shear layer stiffness in the stick region, MPa;

$L$ —is the horizontal length of the shear layer, mm;

$l_n$ —is the length of the stick zone, mm;

$u$ —is the displacement of a point on the shear layer, mm;

$p(x)$ —is the non-uniform normal pressure distribution, N/mm;

$F$ —is the tangential load on the elastic rod, kN;

$\mu$ —is the coefficient of friction

The normal pressure decreases linearly in the direction of the elastic rod as follows:

$$p(x) = p_0 - k_p x \quad (5)$$

In formula:  $P_0$ —is the maximum normal pressure, N/mm;  $k_p$ —is the slope of normal pressure.

From Equations (1) and (2), the boundary condition Equation (3), and the continuity condition (4), the displacements in the stick and slipping regions of the elastic rod are obtained as follows [29]:

$$u(x) = \begin{cases} \frac{\{[\mu k_p(L^2 - l_n^2) + 2\mu P_0(l_n - L)] \cos \theta + 2F\} \coth(\eta l_n)}{2\eta EA} & 0 \leq x \leq l_n \\ a_1 x^3 + a_2 x^2 + a_3 x + a_4 & l_n \leq x \leq L \end{cases} \quad (6)$$

and:

$$a_1 = \frac{-\mu k_p \cos \theta}{6EA}, a_2 = \frac{\mu P_0 \cos \theta}{6EA}, a_3 = \frac{\mu k_p L^2 \cos \theta - 2\mu P_0 L \cos \theta + 2F}{2EA}$$

$$a_4 = \frac{\{[\mu k_p(L^2 - l_n^2) + 2\mu P_0(l_n - L)] \cos \theta + 2F\} \coth(\eta l_n)}{2\eta EA} - \frac{-\mu k_p l_n^3 + 3\mu p_0 l_n^3 + 6l_n F - 6\mu p_0 L l_n + 3\mu k_p L^2 l_n}{6EA}$$

$\eta = \sqrt{\frac{k}{EA}}$ , it is a parameter related to the stiffness of the interface shear layer.

From Equations (1) and (2), the stress continuity equation at the critical point of stick and slip  $x = l_n$  can be obtained [28]:

$$k u(l_n)^- \cos \theta = \mu p(l_n)^+ \cos \theta \quad (7)$$

$F$  that can be obtained by simultaneous Equations (6) and (7):

$$F = \frac{\mu(p_0 - k_p l_n) \tanh(\eta l_n)}{\eta} + \mu p_0(L - l_n) \cos \theta - \frac{\mu k_p(L^2 - l_n^2) \cos \theta}{2} \quad (8)$$

In Equation (8), when  $l_n = L$ , the minimum load at which the microslip occurs can be obtained:

$$F_{\min} = \frac{\mu(p_0 - k_p L) \tanh(\eta L)}{\eta} \quad (9)$$

When  $l_n = 0$ , the maximum tangential force for gross slip can be obtained:

$$F_{\max} = \mu p_0 L \cos \theta - \frac{\mu k_p L^2 \cos \theta}{2} \quad (10)$$

Based on Masing's hypothesis of steady-state cyclic hysteresis response, the force–displacement curves during unloading and reloading can be obtained [30]. Masing's hypothesis holds that the unloading and reloading of the system's steady-state hysteresis response are geometrically similar to the initial force curve, but only amplified twice.

Elastic rod unloading process [31]:

$$\frac{F_A - F_0}{2} = -k_c \left( \frac{u(L)_0 - u(L)_A}{2} + D_c \right) \quad (11)$$

In the formula,  $F_0$  and  $F_A$  are the starting force at unloading and the force during unloading, N;  $u(L)_0$  and  $u(L)_A$  are the initial displacement at unloading and the displacement during unloading, mm.

Reloading process [31]:

$$\frac{F_A + F_0}{2} = -k_c \left( \frac{u(L)_0 + u(L)_A}{2} + D_c \right) \quad (12)$$

Meanwhile

$$k_c = \frac{\eta EA}{\eta(L-l_n) + \coth(\eta l_n)}$$

$$D_c = \left[ 2\mu k_p L^3 - 3\mu p_0 L^2 + \frac{3\mu k_p (L^2 - l_n^2) - 6\mu p_0 (L - l_n)}{\eta \tanh(\eta l_n)} + \right. \\ \left. \mu k_p l_n^3 - 3\mu p_0 l_n^2 - 3\mu k_p L^2 l_n + 6\mu p_0 L l_n \right] / \left[ 6(L - l_n) + \frac{6}{\eta \tanh(\eta l_n)} \right]$$

From Equations (7) and (8), the force–displacement hysteresis curve of the sealing surfaces under cyclic load can be obtained. The area included in the hysteresis curve is the energy dissipation generated by each cycle of cyclic loading [18].

$$\Delta E_h = 4 \int_{l_n}^L \mu p(x) [u(x) - u_n(x)] dx \quad (13)$$

where,  $\Delta E_h$  is the microslip energy dissipation of per cycle, J;  $u_n(x)$  is the critical displacement when the stick region is converted into slip region, mm.

## 2.2. Verification of Dynamic Model

To verify the above model, referring to the sealing surfaces' structure and constraints shown in Figure 4, a FEM of friction contact of the sealing surfaces as shown in Figure 5 is established by ABAQUS. The FEM selects the C3D8I element suitable for the contact analysis. Mesh refinement is applied to particular areas, such as sealing surfaces and shoulder regions, with a mesh size of 0.10. Areas not deemed critical are assigned a relatively rough mesh in order to reduce computational time. Abaqus/Standard Solver is used to analyze finite element models. The interaction attribute is set using the Coulomb friction model to set the contact attribute, the tangential behavior friction formula uses a penalty function, and the normal behavior is set to hard contact [10,32]. Set the Box (rigid body) with higher hardness as the main contact surface and set the Pin (elastic body) as the secondary contact surface. Select a penalty friction formula to simulate a small amount of relative movement during the sticking of the contact surfaces. The left end of the rigid body is set to be fully constrained and a cyclic tangential load is applied at the right end of the elastic body, and a normal pressure is applied at the contact surface. According to the dimensions and material parameters of premium connections and literature [18], the parameters in Table 1 are respectively substituted into the Formulas (11) and (12) and the FEM and the force–displacement hysteresis curves of the two models are calculated (as shown in Figure 6). From the figure, it can be seen that the force–displacement hysteresis curves of both models approximate olive-shaped curves, and the degree of overlap between the two curves is relatively high. Under monotonic loading, the force–displacement curves consist of linear and nonlinear segments. As the load increases, initially, the displacement of both models shows linear increments with nearly the same magnitude. Then, with further increases in load, the displacement increases nonlinearly, with the FEM exhibiting slightly greater increments than the shear layer model, indicating that the FEM dissipates more energy than the shear layer model. The energy dissipation values of the two models are 0.0399 J and 0.0414 J, respectively, with a difference of 3.5%, thus validating the effectiveness of the FEM.

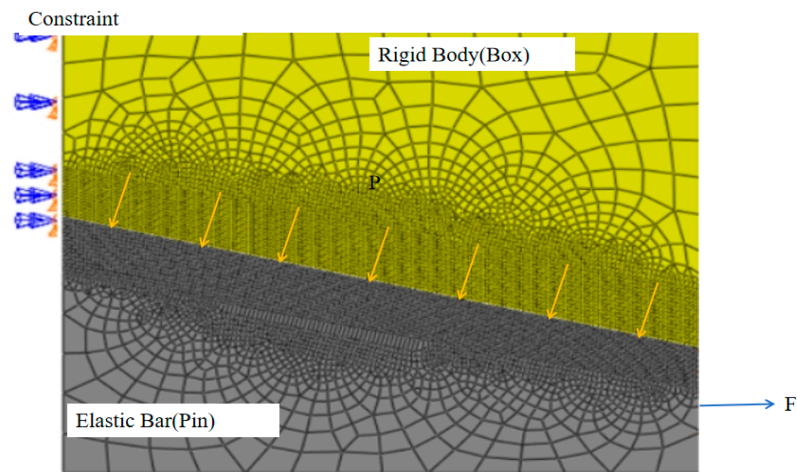


Figure 5. Finite model of friction contact on sealing surfaces.

Table 1. Shear layer model parameters.

Elastic Modulus (GPa)	Cross-Sectional Area of Elastic Rod A (mm <sup>2</sup> )	Shear Layer Stiffness k (GPa)	Sealing Surface Cone Angle $\theta$ (°)	Contact Length of Sealing Surface (mm)	Friction Coefficient ( $\mu$ )	Normal Pressure (N/mm)
210	200	10	13.6	2.67	0.1	$3.1 \times 10^4$

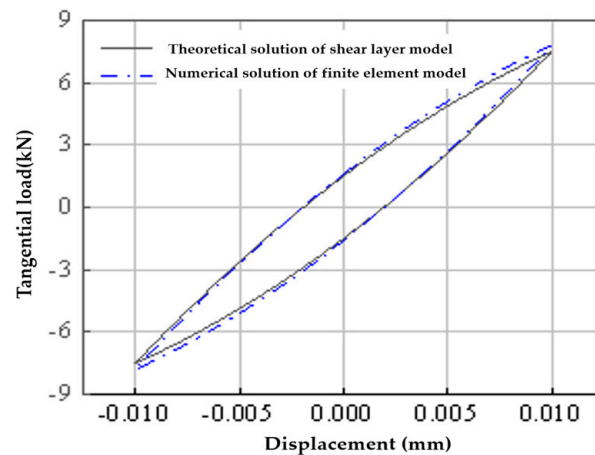
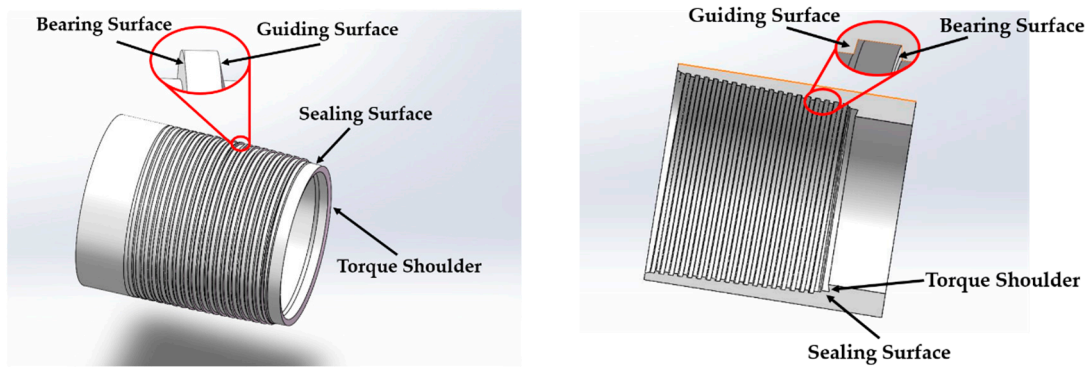


Figure 6. Hysteresis curves of two models.

### 3. FEM of Premium Connection

From the analysis in the previous section, it is known that the energy dissipation of the sealing surfaces is characterized by a force–displacement hysteresis curve, and the effectiveness of using numerical simulation methods to analyze the energy dissipation of the sealing surfaces is verified. In order to study the influence of sealing structure and downhole loads on energy dissipation and sealing performance of premium connections, a friction contact FEM is established in Section 2—a  $\phi 88.9 \times 6.45$  P110 full-size spherical-conical premium connection. As shown in Figure 7, the sealing surface of the coupling part is a 1:16 conical surface, the sealing surface of the tubing end is a spherical surface with a radius of 10 mm, the torque shoulder is  $25^\circ$ , the connection thread bearing angle is  $-3^\circ$ , the guide surface is  $10^\circ$  and the thread taper is 1:16.



**Figure 7.** Solid modal of premium connection.

### 3.1. FEM for Friction Contact

Due to the elastic and plastic deformation of the sealing surfaces and thread under the action of make-up and external loads, it is necessary to enable the geometric nonlinearity and material nonlinearity settings in ABAQUS software. The relevant material parameters for premium connections are shown in Table 2.

**Table 2.** Material parameters of premium connection.

Elastic Modulus	Poisson's Ratio	FrictionCoefficient	Maximum Yield Strength	Strength Limit
210 GPa	0.3	0.1	828 MPa	835 MPa

The C3D8I element is selected for premium connection, and mesh refinement is performed on the threads, sealing surfaces, and torque shoulders, as shown in Figure 8. To accelerate the solution speed of nonlinear analysis and ensure the accuracy of calculation, ABAQUS/Standard solver is selected for solution analysis [33,34].

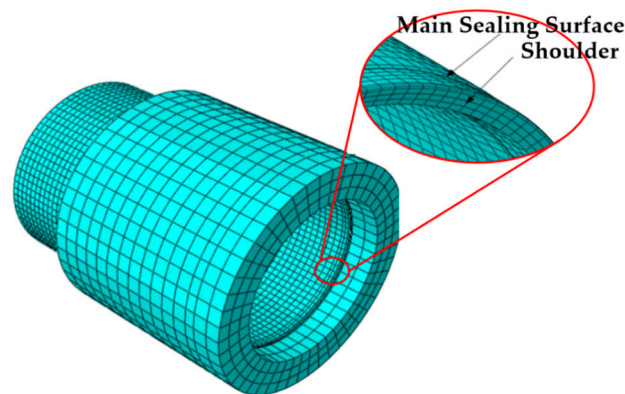


**Figure 8.** Meshed FEM for premium connection.

After make-up, the premium connection's contact includes the threads, sealing surfaces, and torque shoulder. In nonlinear contact analysis, surface-to-surface contact elements are selected and contact pairs are established according to the method in Section 3. As shown in Figure 9, the coupling's face is set with fixed full constraints, a reference point is arranged at the axis position of the tubing and coupled with the face of the tubing to apply an axial cyclic load to the reference point, and a constant internal pressure is applied to the inner wall of the tubing and the coupling.

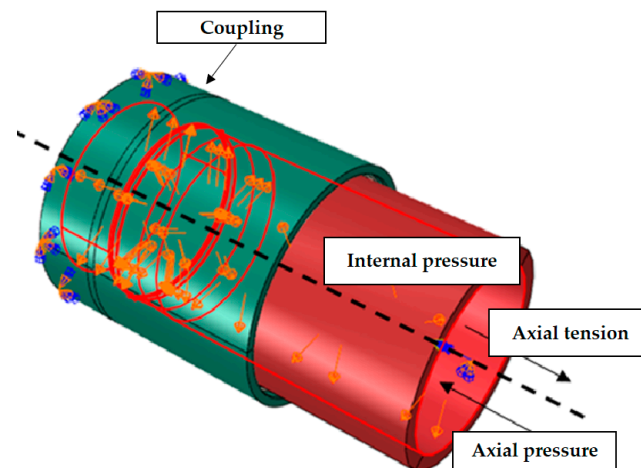


**Figure 9.** Constraint settings for premium connection.

### 3.2. FEM for Vibration

A FEM of tubing with external threads (each tubing is 9.8 m in length) is established and fully constrained at both ends of the tubing to form a vibration model of the tubing string containing the connection. The material parameters, meshing, and contact settings of the FEM refer to Section 2.1. The finite element meshed model is shown in Figure 10.

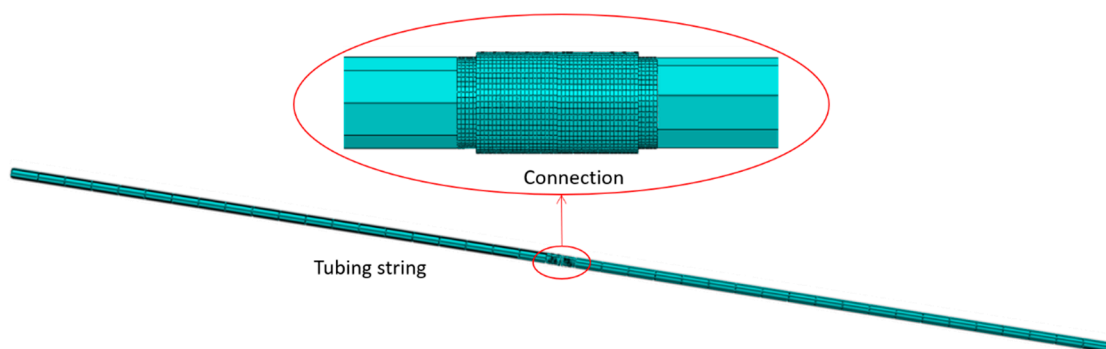


**Figure 10.** FEM of tubing string with connections.

### 3.3. Mesh Independent Verification

In order to minimize the errors in the calculation results caused by the quality and quantity of the mesh during the analysis process, the paper adopts a mesh-independent verification method. At the sealing surface of the premium connection, this article uses C3D8I elements for mesh division, with mesh sizes of 0.05, 0.1, 0.15, 0.2, and 0.25 mm, respectively [35], the maximum Von Mises stress distribution at the sealing surface of the premium connections under the optimal tightening torque is shown in Figure 11. When the mesh size decreases from 0.25 mm to 0.15 mm, the magnitude of the maximum stress increases monotonically from 0 to 2.12%. When the mesh size is between 0.05 and 0.15 mm, the maximum stress change amplitude at the sealing surface is between 4.0 and 4.4%. The results show that when the mesh size is less than 0.15 mm, the change in mesh size has a small impact on the maximum contact stress value at the sealing surface. As in finite element simulation, the smaller the mesh size, the more accurate the convergence of the obtained results. Taking into account the calculation time and efficiency, this paper adopts a mesh size of 0.10 for analysis.

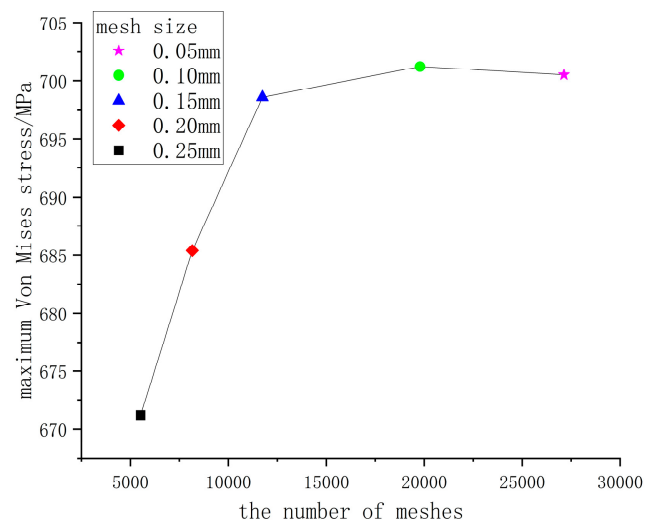


**Figure 11.** The distribution of maximum von Mises stress under different mesh sizes.

#### 4. Result

Structural parameters and load conditions are the main factors affecting the sealing performance of premium connections. For spherical-conical premium connections, the radius determines the initial contact conditions such as the contact area, length, and contact pressure of the sealing surfaces. In addition, the dynamic load and vibration of the downhole string will change the contact state of the sealing surfaces, threatening the sealing performance of the connection. This section considers the influence of the radius of the sealing surfaces, the pressure inside the tubing, the axial force amplitude on the tubing string (As shown in Table 3), and the modal vibration mode under the axial cyclic load as shown in Figure 12. The finite element method is used to analyze the von Mises stress, contact pressure, and force–displacement hysteresis curve, obtaining the energy dissipation and sealing performance of the premium connection under various influencing factors.

**Table 3.** Impact parameters.

	Spherical Radius (mm)	Internal Pressure (MPa)	Cyclic Load Amplitude (kN)
I	10, 15, 20	60	400
II	15	60, 70, 80	400
III	15	60	400, 500, 600

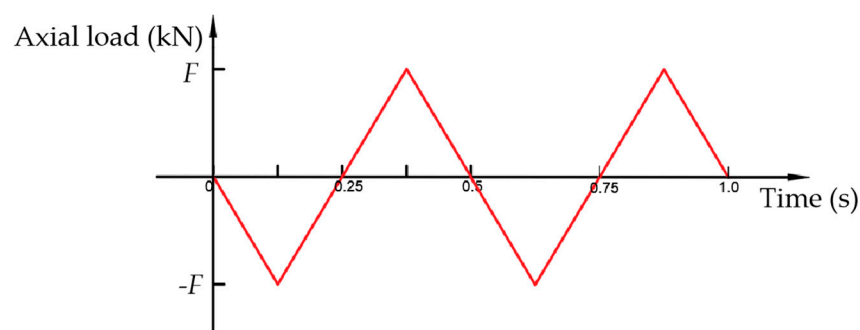


**Figure 12.** Axial cyclic load.

##### 4.1. Effect of Spherical Radius on Energy Dissipation

Figure 13 shows the von Mises stress nephogram of premium connection with different spherical radii under 60 MPa internal pressure and 400 kN axial cyclic load. As can be seen from Figure 13, under axial compression load, there is significant stress concentration at the thread portion of the connection. When the spherical radius is larger than 15 mm, the

maximum von Mises stress of the connection is 834.8 MPa, which is near the strength limit of the material (835 MPa). However, under axial tension load, the overall von Mises stress distribution of the connection is uniform and does not exceed the maximum yield limit of the material (828 MPa). This is because there is a preload at the thread in the axial direction during the make-up of the premium connection. Due to the same axial compression load and preload direction, the von Mises stress in the connection increases, and the stress concentration at the thread is significant.

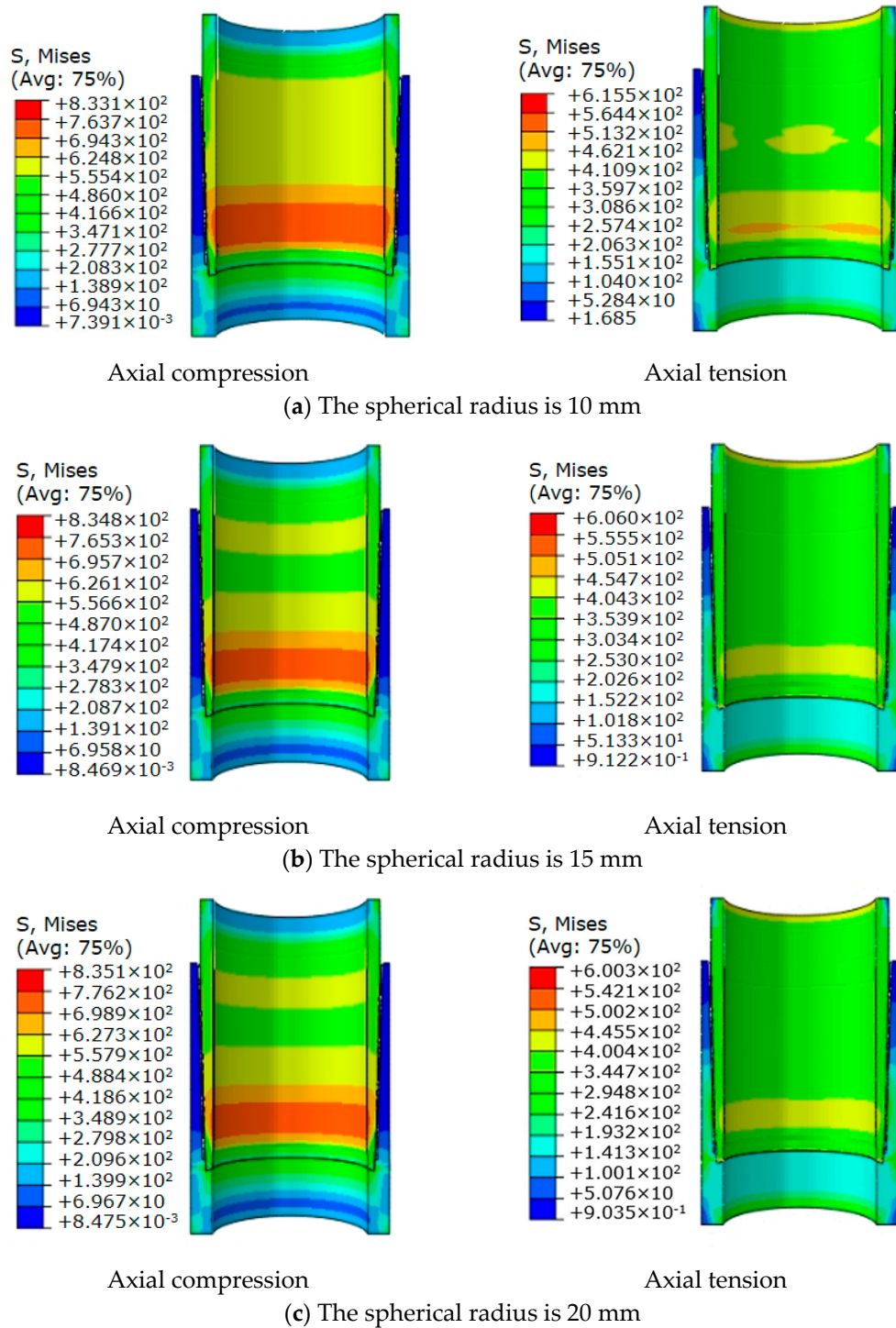


Figure 13. The von Mises stress nephogram for connection with different spherical radii.

Figure 14 shows the contact pressure curves of sealing surfaces with different spherical radii during axial cyclic loading. In the figure, 0–1 s is the internal pressure loading process, and 1 s–2 s is the axial cyclic load loading process. The wave peak is the maximum axial compression load, and the wave trough is the maximum axial tension load. As can be seen from Figure 14, during initial internal pressure loading, the larger the spherical radius, the lower the contact pressure on the sealing surfaces. During the entire axial load cycle, the contact pressure hardly changes with the increase of the spherical radius, and only decreases by 1.8% during axial tension.

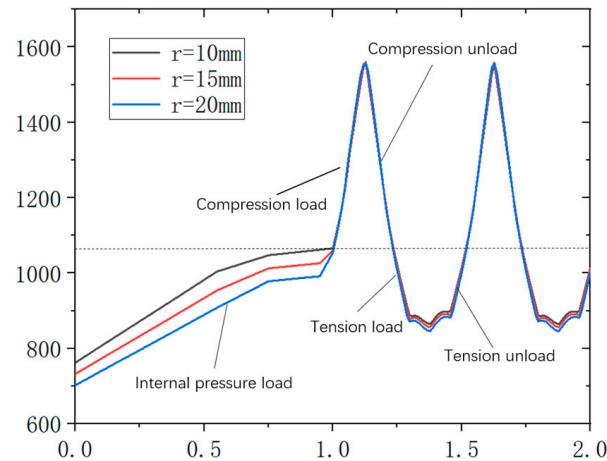


Figure 14. Contact pressure curves at sealing surfaces with different spherical radii.

Extracting the friction force and node displacement at each analysis step on the sealing surfaces within a cycle, the force–displacement hysteresis curves with different spherical radius is obtained as shown in Figure 15, and the gross slip and energy dissipation curves as shown in Figure 16. From Figure 15, it can be seen that the force–displacement hysteresis curve of the spherical-conical seal structure approximates a parallelogram, and its gross slip is much greater than the microslip, indicating that the energy dissipation of the seal structure is mainly caused by gross slip [36].

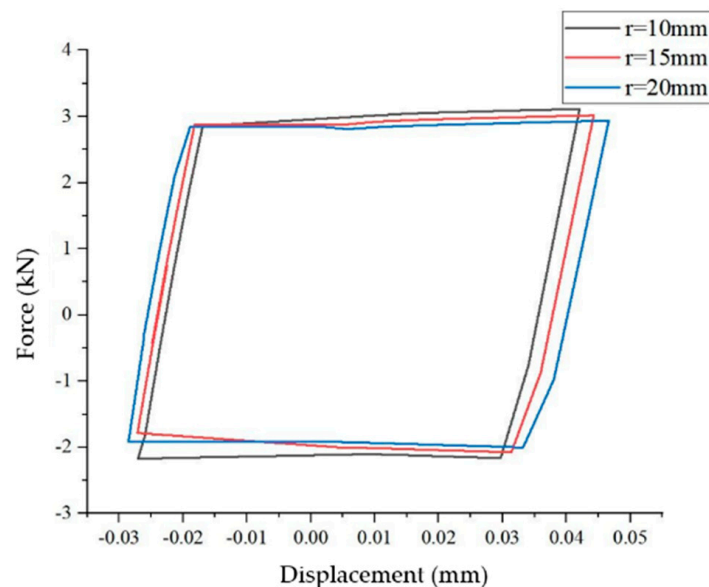
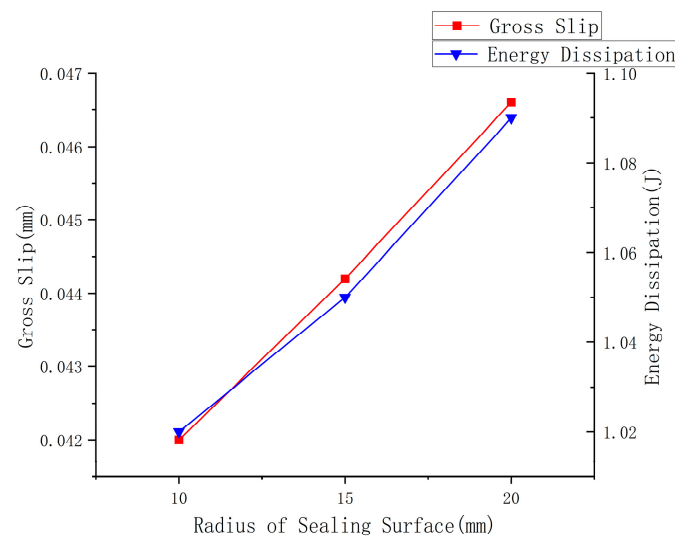


Figure 15. Force–displacement hysteresis curves for different spherical radii.



**Figure 16.** Gross slip and energy dissipation for different spherical radii.

As can be seen from Figure 16, energy dissipation increases as the spherical radius increases. When the spherical radius is increased from 10 mm to 20 mm, the gross slip increases by 5.2% and 5.4%, and the energy dissipation increases by 2.9% and 3.8%, respectively (as shown in Table 4). This is because the larger the spherical radius of the surface, the lower the contact pressure, resulting in a decrease in the friction required for gross slip of the sealing surfaces, and an increase in the amount of gross slip at the connection sealing surfaces. At the same time, since gross slip is the main factor causing energy dissipation, the larger the spherical radius, the greater the energy dissipation value. This will lead to increased wear on the sealing surfaces, which will reduce the sealing performance of the connection.

**Table 4.** Effect of spherical radius on energy dissipation and gross slip.

Spherical Radius (mm)	Gross Slip		Energy Dissipation	
	Value (mm)	Growth Rate (%)	Value (J)	Growth Rate (%)
10	0.0420		1.02	
15	0.0442	5.2	1.05	2.9
20	0.0466	5.4	1.09	3.8

From the above analysis, it can be seen that under the same axial cyclic load, it is difficult to analyze the impact of the spherical radius on the sealing performance of the connection by the contact pressure of the sealing surfaces; however, the energy dissipation theory can effectively solve this problem.

#### 4.2. Effect of Internal Pressure on Energy Dissipation

Figure 17 shows the interaction of 400 kN axial cyclic load with 60 MPa, 70 MPa, and 80 MPa internal pressure. As can be seen from Figure 17, with the increase of internal pressure, the von Mises stress in the connection increases. When the internal pressure is 80 MPa, the maximum von Mises stress of the connection under axial compression load is 844.4 MPa, which exceeds the strength limit of the material. The stress concentration of the thread is a potential danger point.

Figure 18 shows the contact pressure curve of sealing surfaces under the combined action of axial cyclic load and different internal pressures. Table 5 shows the maximum contact pressure of sealing surfaces under different internal pressures. When the internal pressure increases from 60 MPa to 80 MPa, the contact pressure decreases by 0.5% and 4.6%. During the axial compression stage, the contact pressure decreased by 1.5% and 12% respectively (as shown in Table 5). Existing research has shown that the greater the internal

pressure [37], the greater the contact pressure on the sealing surfaces. This is because previous studies were mostly based on statics analysis, ignoring the impact of dynamic loads [38]. From Figure 16, it can be seen that serious plastic deformation has occurred between the thread and the sealing surfaces when the internal pressure is 80 MPa. It can be predicted that under the long-term axial cyclic load, the connection will become loose due to the gradual accumulation of plastic deformation [39], which will lead to a decrease in the contact pressure of the sealing surfaces.

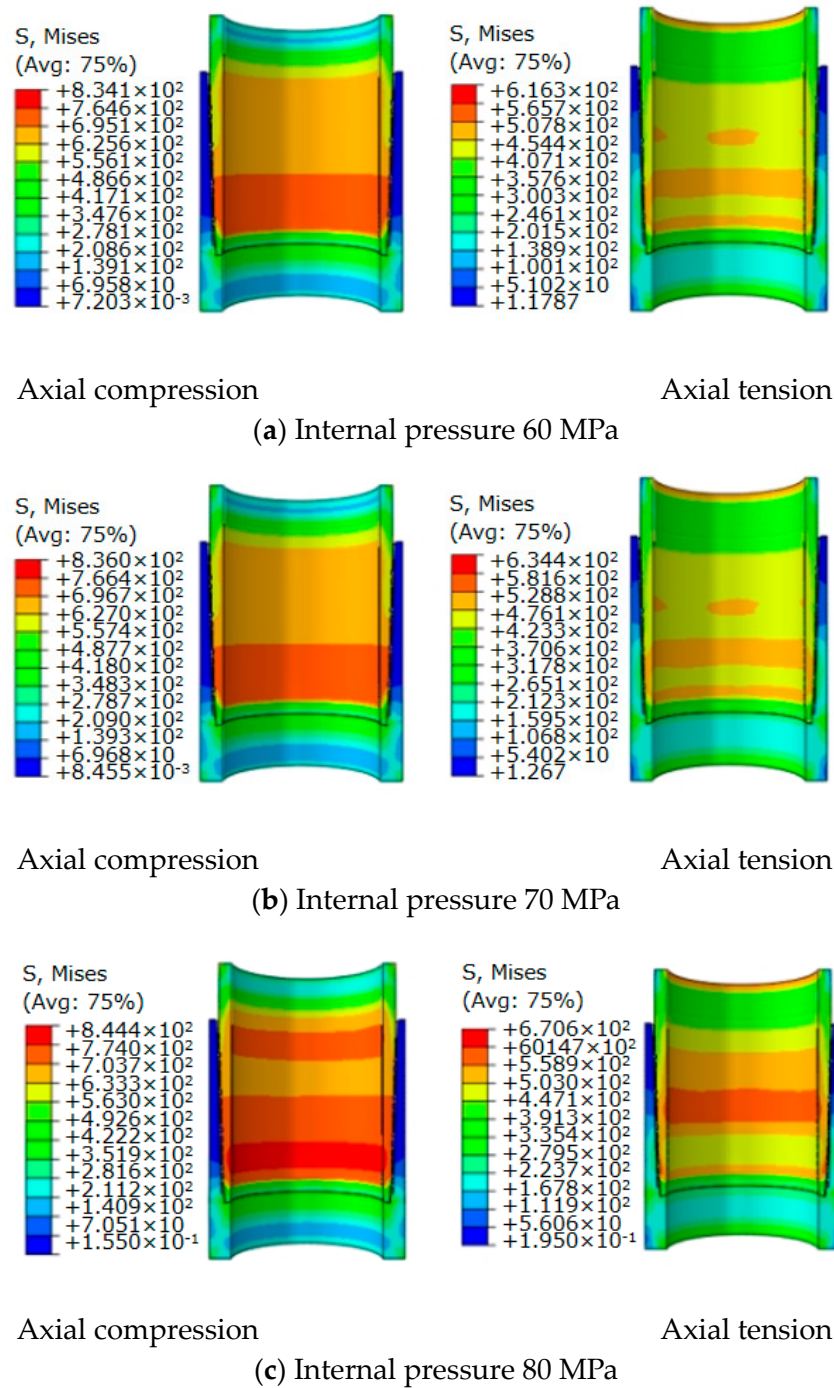
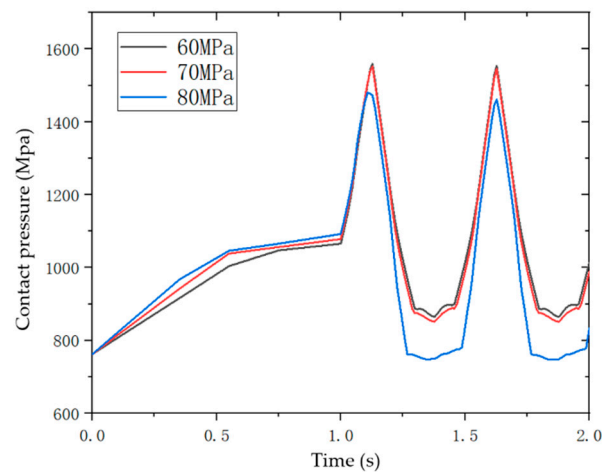


Figure 17. The von Mises stress nephogram of connection under different internal pressures.



**Figure 18.** Contact pressure curve for sealing surfaces under different internal pressures.

**Table 5.** Maximum contact pressure values of sealing surfaces under different internal pressures.

Internal Pressure (MPa)	Maximum Contact Pressure during Axial Compression Stage		Maximum Contact Pressure during Axial Tension Stage	
	Value (MPa)	Growth Rate (%)	Value (MPa)	Growth Rate (%)
60	1559		864.6	
70	1551	−0.5	851.6	−1.5
80	1480.3	−4.6	749.5	−12

Figure 19 is the force–displacement hysteresis curve of the sealing surfaces under the combined action of 400 kN axial cyclic load and different internal pressures. Figure 20 is the corresponding gross slip and energy dissipation curve. It can be seen from Figure 18 that with the increase of internal pressure, the gross slip of sealing surfaces increases, and the energy dissipation increases. The internal pressure increases from 60 MPa to 80 MPa, the gross slip increases by 2.9% and 13.9%, and the energy dissipation increases by 7.8% and 18.2%, respectively (as shown in Table 6). Therefore, when 400 kN axial cyclic load is combined with 80 MPa internal pressure, the energy dissipation of the connection increases significantly, which easily leads to connection loosening and the risk of seal failure exists. In addition, the contact pressure decreases with the loosening of the connection, which explains the decrease of the contact pressure with the increase of internal pressure in the previous section.

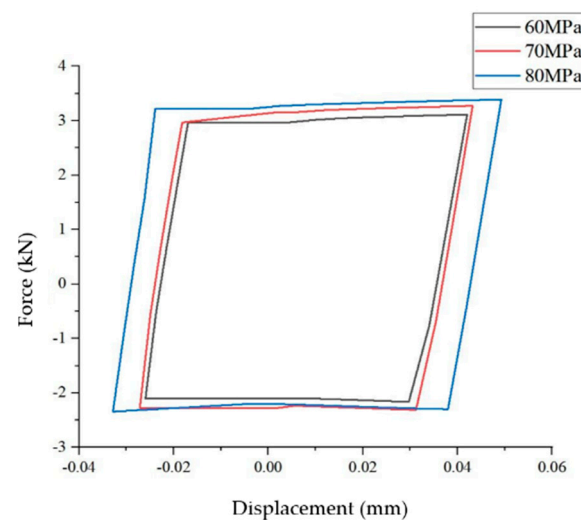


**Figure 19.** Force–displacement hysteresis curve under different internal pressures.

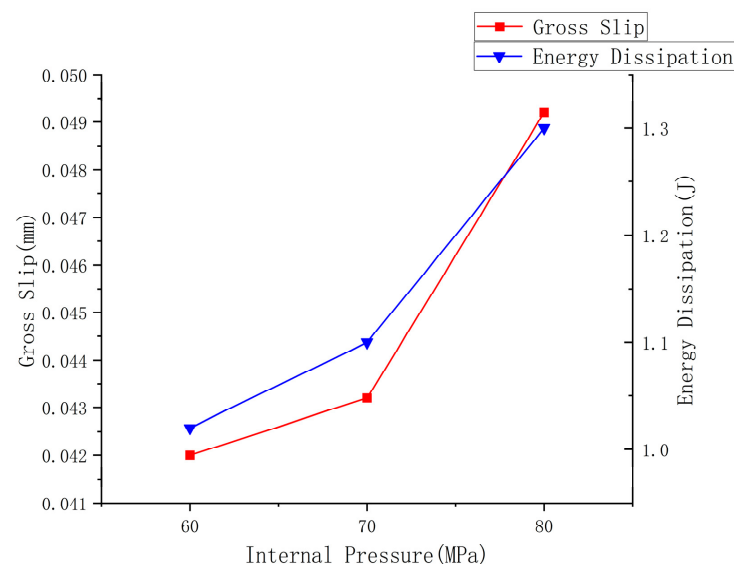


**Figure 20.** Gross slip and energy dissipation curves under different internal pressures.

**Table 6.** Effect of internal pressure on gross slip and energy dissipation.

Internal Pressure (MPa)	Gross Slip		Energy Dissipation	
	Value (mm)	Growth Rate (%)	Value (J)	Growth Rate (%)
60	0.0420		1.02	
70	0.0432	2.9	1.10	7.8
80	0.0492	13.9	1.30	18.2

#### 4.3. Effect of Axial Cyclic Load Amplitude on Energy Dissipation

Figure 21 shows the von Mises stress nephogram of the premium connection under 60 MPa internal pressure combined with 400 kN, 500 kN, and 600 kN axial cyclic load, respectively. It can be seen from Figure 18 that the von Mises stress of connection increases with the increase of axial compressive load amplitude. However, the magnitude of the axial tension load has little effect on the von Mises stress of the connection. When the axial cyclic load is 500 kN, the maximum von Mises stresses of the connection under the axial compressive load are 864.1 MPa, which exceeds the strength limit of the material. Therefore, when the axial cyclic load is greater than 500 kN, the thread stress concentration is a potential risk point.

Figure 22 shows the contact pressure curve of the sealing surfaces under the combined action of internal pressure of 60 MPa and different axial cyclic loads. Table 6 shows the maximum contact pressure of the sealing surfaces under different axial cyclic loads. It can be seen from Figure 22 that the contact pressure on the sealing surfaces decreases with the increase of the axial tension load amplitude. Compression load has little effect on the contact pressure of sealing surfaces. Table 6 shows that the amplitude of the axial tension load increases from 400 kN to 600 kN and the contact pressure decreases by 6% and 6.5%, respectively (As shown in Table 7). This is because, under the action of axial tension, the threaded part of the connection deforms, which causes the displacement of the sealing surfaces and the reduction of interference between the spherical and conical surfaces, finally resulting in the reduction of contact pressure.

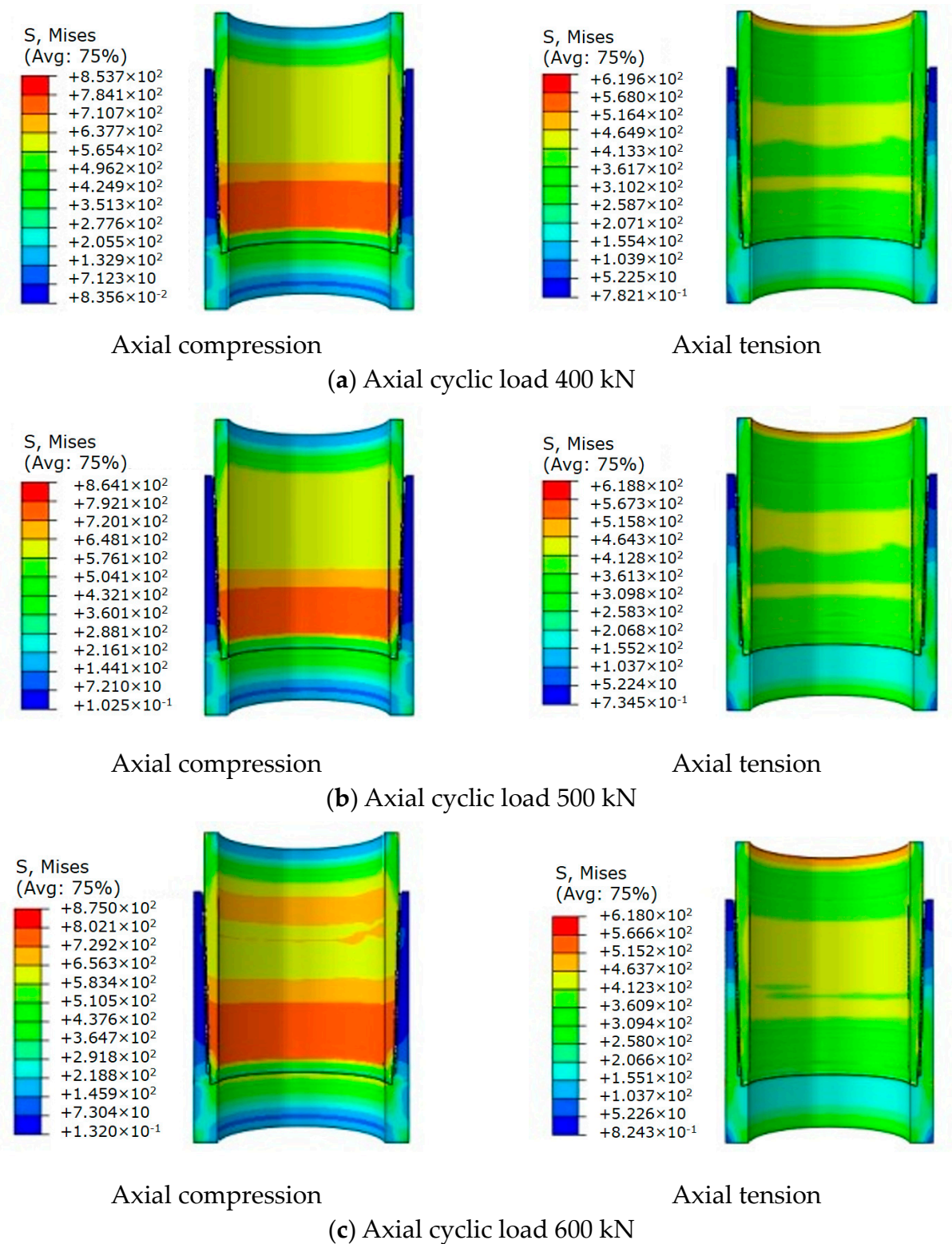
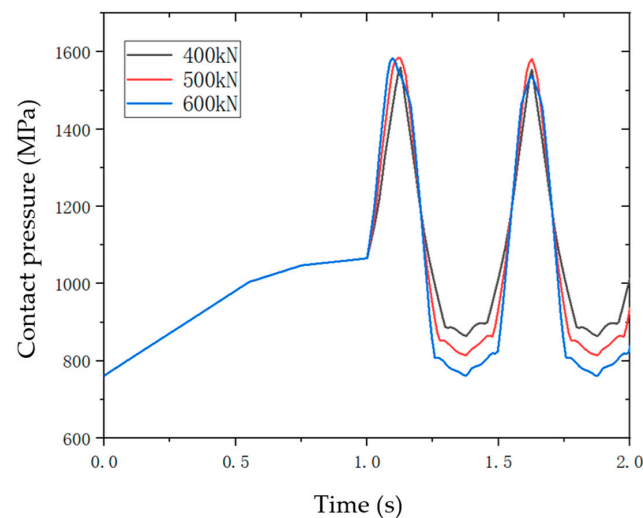


Figure 21. The von Mises stress nephogram of connection under different cyclic loads.



**Figure 22.** Contact pressure curve at the sealing surfaces under different axial cyclic loads.

**Table 7.** Maximum contact pressure of sealing surfaces under different axial cyclic loads.

Axial Cyclic Load (kN)	Maximum Contact Pressure during Axial Compression Stage		Maximum Contact Pressure during Axial Tension Stage	
	Value (MPa)	Growth Rate (%)	Value (MPa)	Growth Rate (%)
400	1559.1		866.5	
500	1583.5	−1.5	814.7	−6
600	1584.3	−0.06	761.4	−6.5

Figure 23 shows the force–displacement hysteresis curve of the sealing surfaces under the combined action of internal pressure of 60 MPa and different axial cyclic loads, and Figure 24 shows the corresponding gross slip and energy dissipation curves. It can be seen from Figure 23 that with the increase of the amplitude of the axial cyclic load, the gross slip of the sealing surfaces increases, and the energy dissipation value increases. The axial tension load increases from 400 kN to 600 kN, the gross slip increases by 39.5% and 27.6%, and the energy dissipation increases by 50% and 25%, respectively (as shown in Table 8). Therefore, when the axial cyclic load is 500 kN, the energy dissipation of the connection increases significantly, which is easy to cause connection sealing failure.

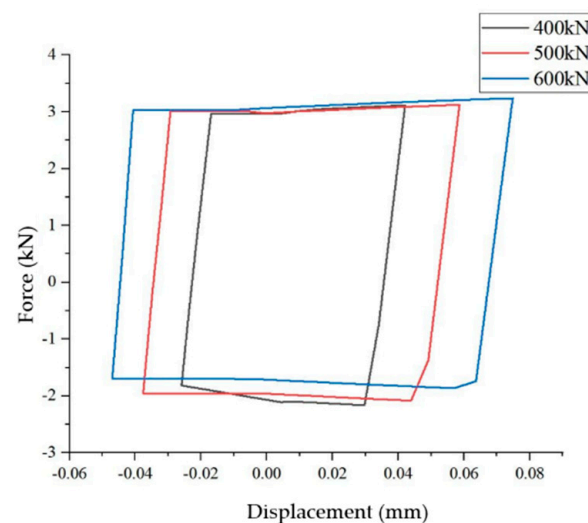


**Figure 23.** Force–displacement hysteresis curves under different axial cyclic loads.

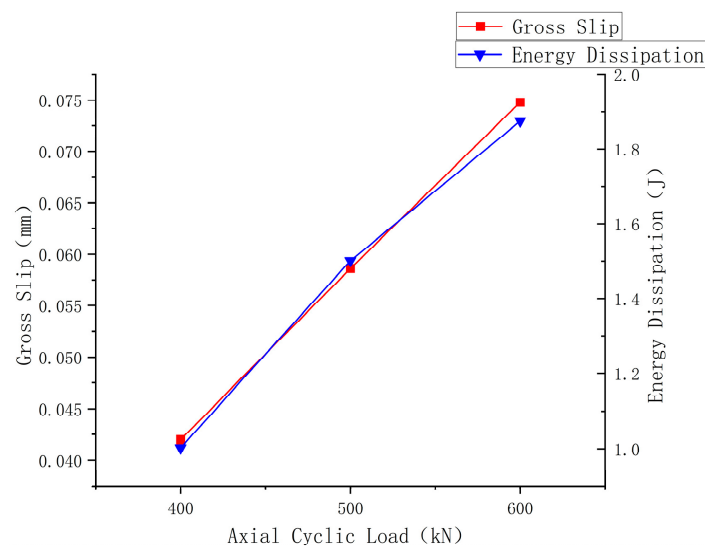


**Figure 24.** Gross slip and energy dissipation under different axial cyclic loads.

**Table 8.** Effect of axial cyclic load on gross slip and energy dissipation.

Axial Cyclic Load (kN)	Gross Slip		Energy Dissipation	
	Value (mm)	Growth Rate (%)	Value (J)	Growth Rate (%)
400	0.0420		1.002	
500	0.0586	39.5	1.501	50
600	0.0748	27.6	1.875	25

Literature [34] assessed the load of sealing failure by using contact pressure. The result shows that there is a risk of sealing failure (up to 95% of the sealing limit) when the load is 60 MPa internal pressure combined with a 600 kN tension load. Compared with the results in this section, the axial load causing sealing failure is larger. This is because the influence of gross slip of sealing surfaces is not considered in the literature [40].

#### 4.4. The Influence of Modal Shapes on Energy Dissipation

First, the modal analysis of the tubing string with premium connection is carried out, and then the modal analysis results are applied as displacement fields to the FEM of the premium connection to obtain the contact pressure and force–displacement hysteresis curves of the sealing surfaces in two vibration cycles. Figure 25 shows the first-order and second-order modes of the premium connection. The modal data of the premium connection are extracted and loaded on the connection in the form of cyclic displacement by editing the ABAQUS input file. Cyclic displacement has two cycles and is divided into 100 incremental steps.

Figure 26 shows the contact pressure nephogram at the sealing surfaces of the connection during two displacement cycles, in which every 0.5 s is a cycle, between 0 s and 0.25 s is the axial compression, and between 0.25 s and 0.5 s is the axial tension. As can be seen from Figure 26, the maximum contact pressure under the first-order mode decreased by 8.7 MPa. The maximum contact pressure under the second-order mode decreased by 8.4 MPa. Due to the fact that the second-order modal shape is smaller than the first-order modal shape, the contact pressure at the sealing surfaces decreases with the increase of the vibration mode order.

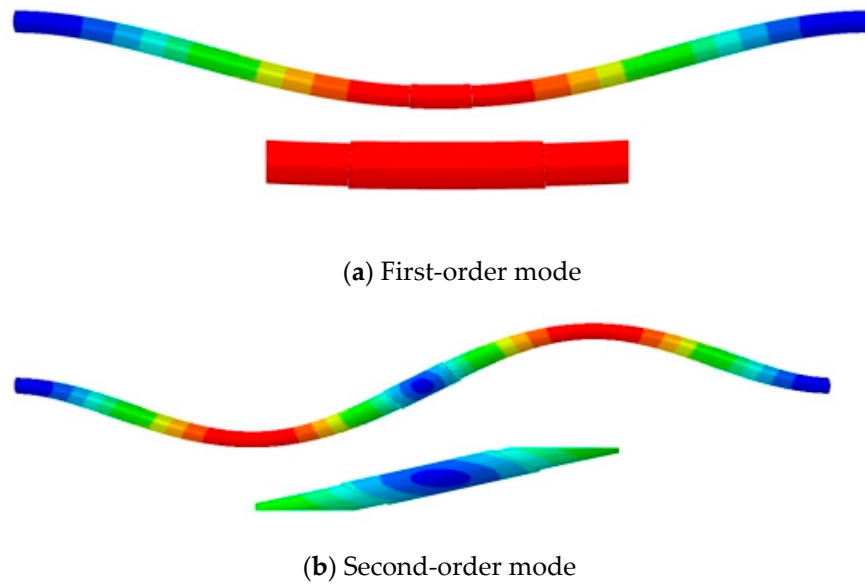


Figure 25. Mode of premium connection.

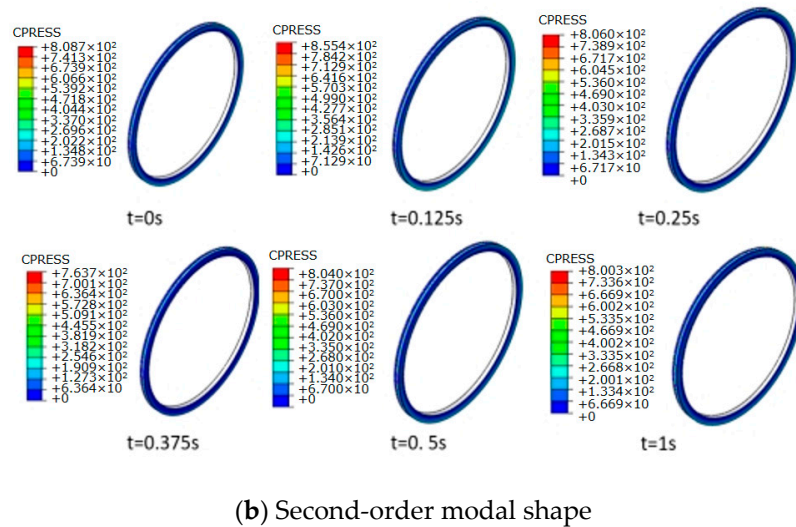
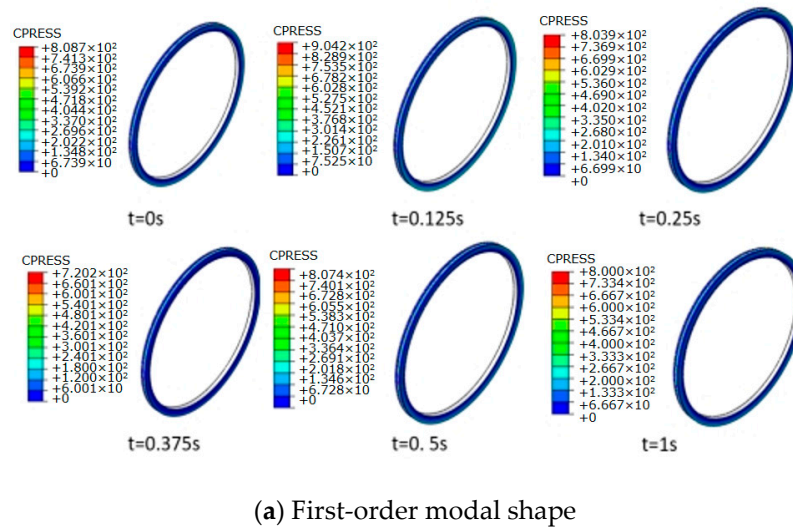
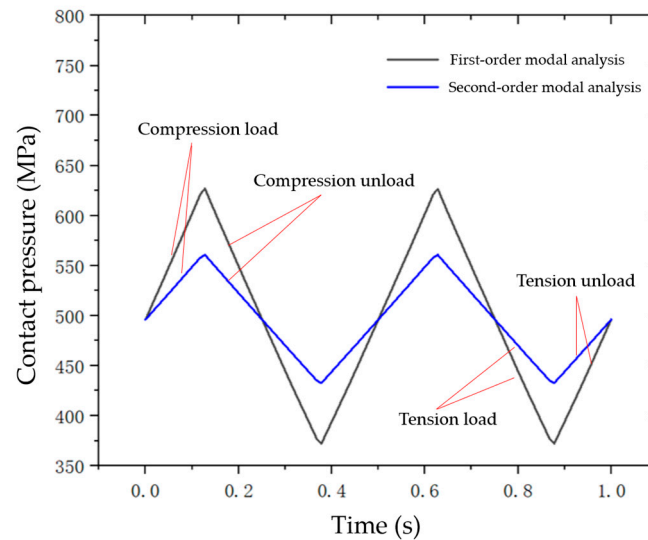


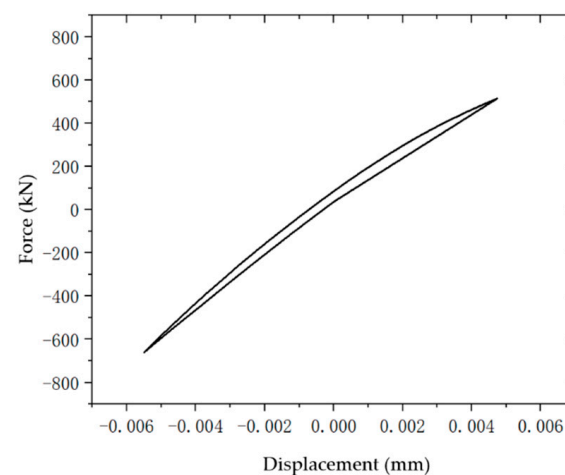
Figure 26. Nephogram of contact pressure on sealing surface under different modal shapes.

Figure 27 shows the average contact pressure curve of the sealing surfaces. It can be seen from the figure that the average contact pressure gradually decreases with the increase of the cycle, and the variation amplitude of the average contact pressure under the first-order mode is greater than that under the second-order mode. This phenomenon is also caused by the fact that the second-order modal shape is smaller than the first-order modal shape.



**Figure 27.** Average contact pressure of sealing surface under different modal shapes.

Extracting the friction force and node displacement of each analysis step within a cycle to obtain the force–displacement hysteresis curve shown in Figure 28. As can be seen from Figure 29, under the vibration modal shape, the force–displacement curve at the sealing surfaces of the spherical-conical premium connection presents a needle-like shape, and there is almost no gross slip of the sealing surfaces. According to Mindlin’s [30] theory, the contact edge of the sealing surfaces undergoes microslip and the center of the sealing surfaces is still in the stick state. Due to the fact that the amplitude of the contact pressure change on the sealing surfaces under the first-order mode is greater than that under the second-order mode (Figure 27), and according to Formula (13), it is known that the normal pressure  $p(x)$  is positively correlated with the energy dissipation, resulting in the energy dissipation under the first-order mode being greater than that under the second-order mode.



**Figure 28.** Force–displacement hysteresis curve under first-order modal shape.

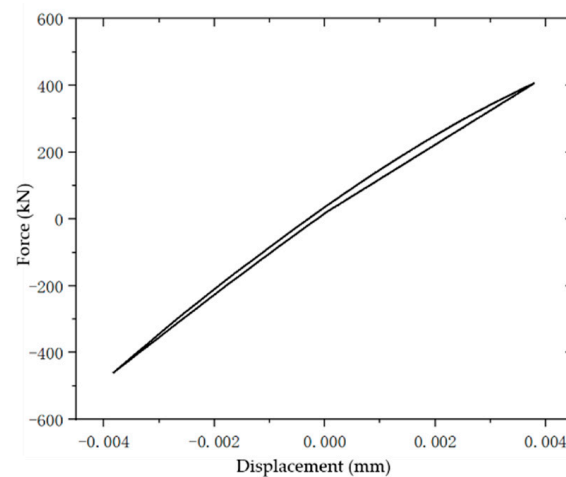


**Figure 29.** Force–displacement hysteresis curve under second-order modal shape.

Compared with the force–displacement curve of the connection sealing surfaces under axial cyclic load (Figure 15, Figure 19, and Figure 23), only stick-slip occurs on the sealing surfaces under the first-order and the second-order modes and the energy dissipation value is minimal (the difference between these is  $10^2$  orders of magnitude). This indicates that the dynamic load caused by changes in fluid pressure and flow rate in the tubing has a greater impact on the sealing performance of the connection than the impact of string vibration.

## 5. Discussion

Through the aforementioned research, it can be found that the method of analyzing the contact pressure of the sealing surface of premium connections under dynamic loading does not effectively explain the decline of connection sealing performance. Firstly, the change in spherical radius under dynamic loading has an insignificant impact on the contact pressure of the sealing surface. Secondly, although internal pressure and contact pressure are positively correlated, the conclusion drawn from traditional analysis methods is that higher internal pressure leads to better sealing performance, contrary to practical situations. It is obvious that all materials have limited strength, exceeding which failure occurs and leads to seal degradation under excessive loading. The method of analyzing the sealing performance of connections using energy dissipation in this article can explain this issue. For spherical-conical premium connections, the gross slip of the sealing surfaces under dynamic load and the microslip of the sealing surfaces under modal vibration mode are analyzed. Both types of slip mentioned above will generate energy dissipation, leading to a decrease in sealing performance.

However, there are still numerous unresolved issues regarding the energy dissipation and sealing performance of premium connections, in particular, the lack of experimental verification. The sealing surfaces of premium connections are typically located in a completely enclosed structure, making it difficult to directly measure the contact pressure and sliding length of the sealing surfaces. This makes it difficult to obtain the force–displacement hysteresis curve of the sealing surfaces. When the tubing string is working downhole, there is liquid or gas in the tubing string, and there is repeated momentum and energy exchange at the interface between the fluid and the tubing string, resulting in fluid–structure interaction excitation, which increases the difficulty of the modal analysis of connections. In addition, the relative slip between the sealing surfaces not only generates energy dissipation but also causes wear, further impacting the sealing performance of the connections. In future studies, the accuracy of FEM analysis will be further validated through force–displacement experiments on connections.

The main purpose of this paper is to propose a novel analytical method for evaluating the sealing performance of a premium connection. This method takes into account the dynamic loads and modal shapes and utilizes finite element analysis to obtain the

force-displacement hysteresis curve of the sealing surface. Through analyzing the slip status and energy dissipation of the connection, the impact of dynamic loads on the sealing performance is revealed. The accuracy of the FEM is preliminarily validated by the vibration equation of the rod. The research results can guide the design, manufacturing, inspection, quality control, and production parameter optimization of the premium connections to ensure their sealing performance. In addition, the results can be applied to the production of oil with a high wax content and production processes in difficult conditions [41]. In future research, finite element simulation will be combined with physical experiments to conduct a more in-depth analysis.

## 6. Conclusions

Based on the dynamic model of sealing surfaces, a spherical-conical premium connection FEM is established to analyze the influence laws of connection energy dissipation and sealing performance under different spherical radii, internal pressure, axial cyclic load amplitude, and mode vibration. The results show that the energy dissipation theory can effectively explain the sealing failure of premium connections under dynamic load. The main conclusions are as follows:

- (1) The force–displacement curve of the spherical-conical premium connection under dynamic load is similar to a parallelogram, and its energy dissipation is mainly caused by gross slip. The force–displacement curve under the modal vibration mode assumes a needle-like shape, and its energy dissipation is mainly caused by microslip. Compared with dynamic load, the energy dissipation value of the sealing surfaces under the first-order, the second-order modes is minimal. Therefore, the dynamic load impact on the sealing performance of the connection is greater than string vibration.
- (2) During the cyclic load, the spherical radius is positively correlated with energy dissipation but has little impact on the contact pressure of the sealing surfaces. Under the same axial cyclic load, it is impossible to analyze the influence of spherical radius on the sealing performance of connections by contact pressure, but the energy dissipation theory can effectively solve this problem.
- (3) Under different cyclic loads, the change amplitude of contact pressure is much smaller than that of energy dissipation. When analyzing the influence of cyclic load amplitude on the sealing performance of connections, the results tend to be conservative in terms of the contact pressure of sealing surfaces.
- (4) Under the combined action of internal pressure and axial cyclic load, it will cause plastic deformation accumulation on the thread and sealing surfaces. When the internal pressure and axial cyclic loads are 80 MPa, 400 kN, or 60 MPa, 500 kN, respectively, the thread with stress concentration is a potential danger point. At the same time, the energy dissipation significantly increases, leading to a decline in the sealing performance of the connection which has a risk of sealing failure.

**Author Contributions:** Conceptualization, Y.Y. and Z.Q.; methodology, Y.Y. and Z.Q.; software, Y.Y. and Y.C.; validation, Y.C. and Y.D.; formal analysis, Y.Y.; investigation, Z.W.; resources, Y.Y.; data curation, Z.W.; writing—original draft preparation, Y.Y.; writing—review and editing, Y.Y., Z.Q., Y.C. and Y.D.; visualization, Y.Y.; supervision, Z.Q. and Y.D.; project administration, Y.Y.; funding acquisition, Z.Q. and Y.D. All authors have read and agreed to the published version of the manuscript.

**Funding:** This research was funded by the National Natural Science Foundation of China (NSFC) (Nos. 52274006 and 51974246), and the Natural Science Basic Research Program of Shaanxi (No. 2023-JC-YB-337).

**Institutional Review Board Statement:** Not applicable.

**Informed Consent Statement:** Informed consent was obtained from all subjects involved in the study.

**Data Availability Statement:** The data presented in this study are available on request from the corresponding author.

**Conflicts of Interest:** The authors declare no conflict of interest.

### Nomenclature

$E$	Young's modulus, Gpa
$A$	constant cross-section area of the elastic bar, mm <sup>2</sup>
$\theta$	the taper of the sealing surface, °
$k$	the shear layer stiffness in the stick region, MPa
$L$	the horizontal length of the shear layer, mm
$l_n$	the length of the stick zone, mm
$u$	the displacement of a point on the shear layer, mm
$u'$	the velocity of a point on the shear layer, mm/s
$u''$	the acceleration of a point on the shear layer, mm/s <sup>2</sup>
$p(x)$	the non-uniform normal pressure distribution, N/mm
$F$	the tangential load on the elastic rod, kN
$\mu$	the coefficient of friction
$P_0$	the maximum normal pressure, N/mm
$k_p$	the slope of normal pressure
$F_0$	the starting force at unloading, N
$F_A$	the force during unloading, N
$u(L)_0$	the initial displacement at unloading, mm
$u(L)_A$	the displacement during unloading, mm
$\Delta E_h$	the microslip energy dissipation per cycle, J
$u_n(x)$	the critical displacement when the stick region is converted into slip region, mm

### References

1. Matthews, C. Assessing tubular connection leakage integrity. *World Oil* **2002**, *223*, 82–84.
2. Dou, Y.H.; Cao, Y.P.; Zhang, F.X.; Yang, X.T. Analysis of Influence to the Connect and Seal Ability of Tubing Connection of Inner Pressures. In Proceedings of the Advanced Materials Research, Xi'an, China, 7–8 January 2012; pp. 790–793.
3. Bradley, A.; Nagasaku, S.; Verger, E. Premium connection design, testing, and installation for HPHT sour wells. In Proceedings of the SPE High Pressure/High Temperature Sour Well Design Applied Technology Workshop, The Woodlands, TX, USA, 17–19 May 2005.
4. Xie, J. Numerical evaluation of tubular connections for HPHT applications. In Proceedings of the Baosteel Conference, Shanghai, China, 4–6 June 2013.
5. Li, D.; Botto, D.; Li, R.; Xu, C.; Zhang, W. Experimental and theoretical studies on friction contact of bolted joint interfaces. *Int. J. Mech. Sci.* **2022**, *236*, 107773. [[CrossRef](#)]
6. Xu, H.; Yang, B.; Zhang, Z.; Shi, T. Special considerations to calculate joint strength of premium connections. *J. Pet. Sci. Eng.* **2019**, *182*, 106295. [[CrossRef](#)]
7. Xu, H.; Zhang, Z.; Xiang, S.; Yang, B.; Shi, T. Leakage Model of Tubing and Casing Premium Connection Based on Sinusoidal Contact Simulation between Rough Surfaces. *Processes* **2023**, *11*, 570. [[CrossRef](#)]
8. Yang, B.; Xu, H.; Xiang, S.; Zhang, Z.; Su, K.; Yang, Y. Effects of Make-Up Torque on the Sealability of Sphere-Type Premium Connection for Tubing and Casing Strings. *Processes* **2023**, *11*, 256. [[CrossRef](#)]
9. Nasraoui, M.T.; Chakhari, J.; Khalfi, B.; Nasri, M. Modeling and analysis of a bolted joint under tension and shear loads. *Trans. Can. Soc. Mech. Eng.* **2019**, *43*, 376–386. [[CrossRef](#)]
10. Xu, H.; Yang, B. A Quantitative Model to Calculate Gas Sealing Capacity and Design Sealing Parameters for Premium Connection. *Math. Probl. Eng.* **2020**, *2020*, 9074381. [[CrossRef](#)]
11. Zhiqian, X.; Xiangzhen, Y.; Xiujuan, Y.; Xiaokang, Y.; Mingda, W.; Xiaoyun, Z. Application of micro-leakage mechanism for evaluating the sealing performance of non-API casing connections. *Acta Pet. Sin.* **2014**, *35*, 963.
12. Chen, W.; Di, Q.; Zhang, H.; Chen, F.; Wang, W. The sealing mechanism of tubing and casing premium threaded connections under complex loads. *J. Pet. Sci. Eng.* **2018**, *171*, 724–730. [[CrossRef](#)]
13. Chen, S.-J.; An, Q.; Zhang, Y.; Gao, L.-X.; Li, Q. Loading analysis on the thread teeth in cylindrical pipe thread connection. *J. Press. Vessel Technol.* **2010**, *132*, 031202. [[CrossRef](#)]
14. Wang, Y.; Fan, H.; Zhang, L.; Wei, F.; Feng, G.; Niu, M. Lateral Vibration and Stability of High Temperature and High Pressure Gas Well Test String. *Pet. Mach.* **2011**, *39*, 36–38.
15. Liu, E.; Wang, X.; Zhao, W.; Su, Z.; Chen, Q. Analysis and research on pipeline vibration of a natural gas compressor station and vibration reduction measures. *Energy Fuels* **2020**, *35*, 479–492. [[CrossRef](#)]
16. Luo, J.; Zhang, K.; Liu, J.; Mu, L.; Wang, F. The Study of Tubing Vibration Mechanism in High Pressure Gas Well. *World J. Eng. Technol.* **2021**, *9*, 128. [[CrossRef](#)]
17. Segalman, D.J. A Four-Parameter Iwan Model for Lap-Type Joints. *J. Appl. Mech.* **2005**, *72*, 752–760. [[CrossRef](#)]

18. Sun, D.; Liao, R. Investigation Into the Effect of Interface Characteristics on the Energy Dissipation of the Bolted Joints. *J. Comput. Theor. Nanosci.* **2015**, *12*, 2821–2829. [[CrossRef](#)]
19. Wang, D.; Zhang, Z. A four-parameter model for nonlinear stiffness of a bolted joint with non-Gaussian surfaces. *Acta Mech.* **2020**, *231*, 1963–1976. [[CrossRef](#)]
20. Segalman, D.J. Modelling joint friction in structural dynamics. *Struct. Control Health Monit.* **2006**, *13*, 430–453. [[CrossRef](#)]
21. Tan, L.; Wang, C.; Liu, Y.; Sun, W.; Zhang, W. Study on hysteresis and threaded fitting behavior of bolted joint with non-parallel bearing surface. *Mech. Syst. Signal Process.* **2022**, *168*, 108655. [[CrossRef](#)]
22. Oldfield, M.; Ouyang, H.; Mottershead, J.E. Simplified models of bolted joints under harmonic loading. *Comput. Struct.* **2005**, *84*, 25–33. [[CrossRef](#)]
23. Iwan, W.D. On a Class of Models for the Yielding Behavior of Continuous and Composite Systems. *J. Appl. Mech.* **1967**, *34*, 612–617. [[CrossRef](#)]
24. Wang, S.-A.; Zhu, M.; Xie, X.; Li, B.; Liang, T.-X.; Shao, Z.-Q.; Liu, Y.-L. Finite Element Analysis of Elastoplastic Elements in the Iwan Model of Bolted Joints. *Materials* **2022**, *15*, 5817. [[CrossRef](#)] [[PubMed](#)]
25. Xueliang, Z.; Yumei, H.; Weiping, F.; Xiaoyue, W.; Yongchao, L. Research on the Normal Damping of Machine Joints. In Proceedings of the International Design Engineering Technical Conferences and Computers and Information in Engineering Conference, Atlanta, GA, USA, 13–16 September 1998.
26. Fu, W.; Huang, Y.; Zhang, X.; Guo, Q. Experimental investigation of dynamic normal characteristics of machined joint surfaces. *J. Vib. Acoust.* **2000**, *122*, 393–398. [[CrossRef](#)]
27. Yang, Y.; Zhan, Q.; Yihua, D.; Yinping, C. Analysis of Energy Dissipation on the Sealing Surface of Premium Connection Based on a Microslip Shear Layer Model. *Energies* **2022**, *15*, 8400.
28. Yu, Y.; Qu, Z.; Cao, Y.; Dou, Y.; Li, J. Sealability Analyses of Premium Connections Characterized by a Surface Fractal Function. *Appl. Sci.* **2023**, *13*, 6467. [[CrossRef](#)]
29. Menq, C.-H.; Griffin, J.; Bielak, J. The influence of microslip on vibratory response, part II: A comparison with experimental results. *J. Sound Vib.* **1986**, *107*, 295–307. [[CrossRef](#)]
30. Menq, C.H.; Bielak, J.; Griffin, J.H. The influence of microslip on vibratory response, part I: A new microslip model. *J. Sound Vib.* **1986**, *107*, 279–293. [[CrossRef](#)]
31. Zhang, X.; Huang, Y.; Wen, S. Fractal model of contact stiffness of joint surfaces. *Trans. Chin. Soc. Agric. Mach.* **2000**, *31*, 89–91.
32. Izumi, S.; Yokoyama, T.; Iwasaki, A.; Sakai, S. Three-dimensional Finite Element Analysis on Tightening and Loosening Mechanism of Bolted Joint. *Trans. Jpn. Soc. Mech. Eng. Ser. A* **2005**, *71*, 204–212. [[CrossRef](#)]
33. Guangjie, Y.; Zhenqiang, Y.; Qinghua, W.; Zhentong, T. Numerical and experimental distribution of temperature and stress fields in API round threaded connection. *Eng. Fail. Anal.* **2006**, *13*, 1275–1284. [[CrossRef](#)]
34. Shen, X.P.; Shen, G.Y. Numerical Analysis on the Expanding Process of Expandable Casing and Contact Evaluation of Its Threaded Connection. In Proceedings of the Applied Mechanics and Materials, Hong Kong, China, 17–18 August 2013; pp. 632–638.
35. Nagata, S.; Fujita, S.; Sawa, T. FEM Stress Analysis and Leakage Behavior of Pipe-Socket Threaded Joints Subjected to Bending Moment and Internal Pressure. In Proceedings of the ASME 2020 Pressure Vessels & Piping Conference, Virtual, Online, 3 August 2020.
36. Song, Y.; McFarland, D.M.; Bergman, L.A.; Vakakis, A.F. Effect of pressure distribution on energy dissipation in a mechanical lap joint. *AIAA J.* **2005**, *43*, 420–425. [[CrossRef](#)]
37. Murtagian, G.; Fanelli, V.; Villasante, J.; Johnson, D.; Ernst, H. Sealability of stationary metal-to-metal seals. *J. Trib.* **2004**, *126*, 591–596. [[CrossRef](#)]
38. Ferjaoui, A.; Yue, T.; Wahab, M.A.; Hojjati-Talemi, R. Prediction of fretting fatigue crack initiation in double lap bolted joint using Continuum Damage Mechanics. *Int. J. Fatigue* **2015**, *73*, 66–76. [[CrossRef](#)]
39. Dou, Y.; Li, Y.; Cao, Y.; Yu, Y.; Zhang, J.; Zhang, L. FE simulation of sealing ability for premium connection based on ISO 13679 CAL IV tests. *Int. J. Struct. Integr.* **2020**, *12*, 138–148. [[CrossRef](#)]
40. Ilyushin, Y.V.; Novozhilov, I. Temperature field control of a metal oil-well tubing for producing of high-paraffin oil. In Proceedings of the 2020 XXIII International Conference on Soft Computing and Measurements (SCM), St. Petersburg, Russia, 27–29 May 2020; pp. 149–152.
41. Martirosyan, A.V.; Kukharova, T.V.; Fedorov, M.S. Research of the Hydrogeological Objects' Connection Peculiarities. In Proceedings of the 2021 IV International Conference on Control in Technical Systems (CTS), Saint Petersburg, Russia, 21–23 September 2021; pp. 34–38.

**Disclaimer/Publisher's Note:** The statements, opinions and data contained in all publications are solely those of the individual author(s) and contributor(s) and not of MDPI and/or the editor(s). MDPI and/or the editor(s) disclaim responsibility for any injury to people or property resulting from any ideas, methods, instructions or products referred to in the content.